Journal of Geophysical Research: Earth Surface

Supporting Information for

Controls on water storage and drainage in crevasses on the Greenland Ice Sheet

T. R. Chudley[1]*, P. Christoffersen[1], S. H. Doyle[2], T. P. F. Dowling[3†], R. Law[1], C. M. Schoonman[1‡], M. Bougamont[1], and B. Hubbard[2]

[1] Scott Polar Research Institute, University of Cambridge

[2] Centre for Glaciology, Department of Geography and Earth Sciences, Aberystwyth University

[3] Department of Geography, King's College London

* Corresponding author: Tom Chudley (trc33@cam.ac.uk)

[†] Now at the National Centre for Earth Observation, University of Leicester,Department of Physics & Astronomy, University Road, Leicester, LE1 7RH, United Kingdom.

[‡] Now at the Alfred Wegener Institute Helmholtz Centre for Polar and Marine Research, Bremerhaven, Germany.

Contents of this file

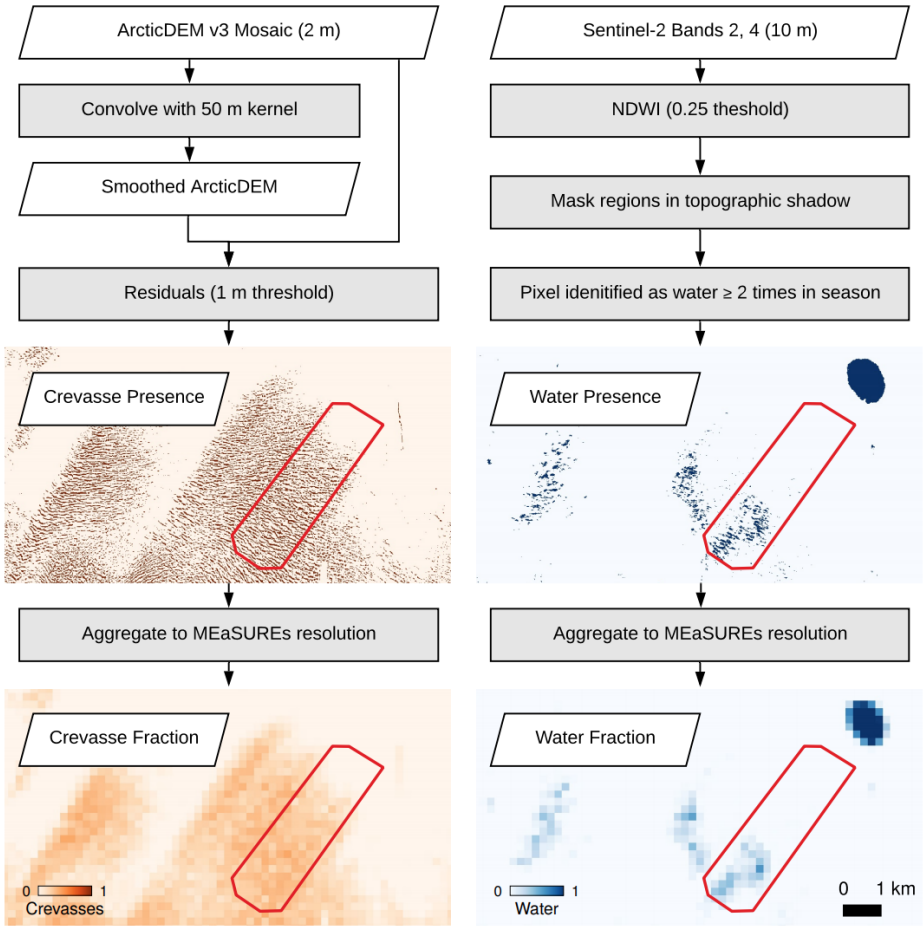

Figure S1. Flow diagram visualising the production of crevasse fraction data from ArcticDEM (left) and water fraction data from Sentinel-2 optical imagery (right). Red box outlined in maps marks the extent of the UAV ROI.

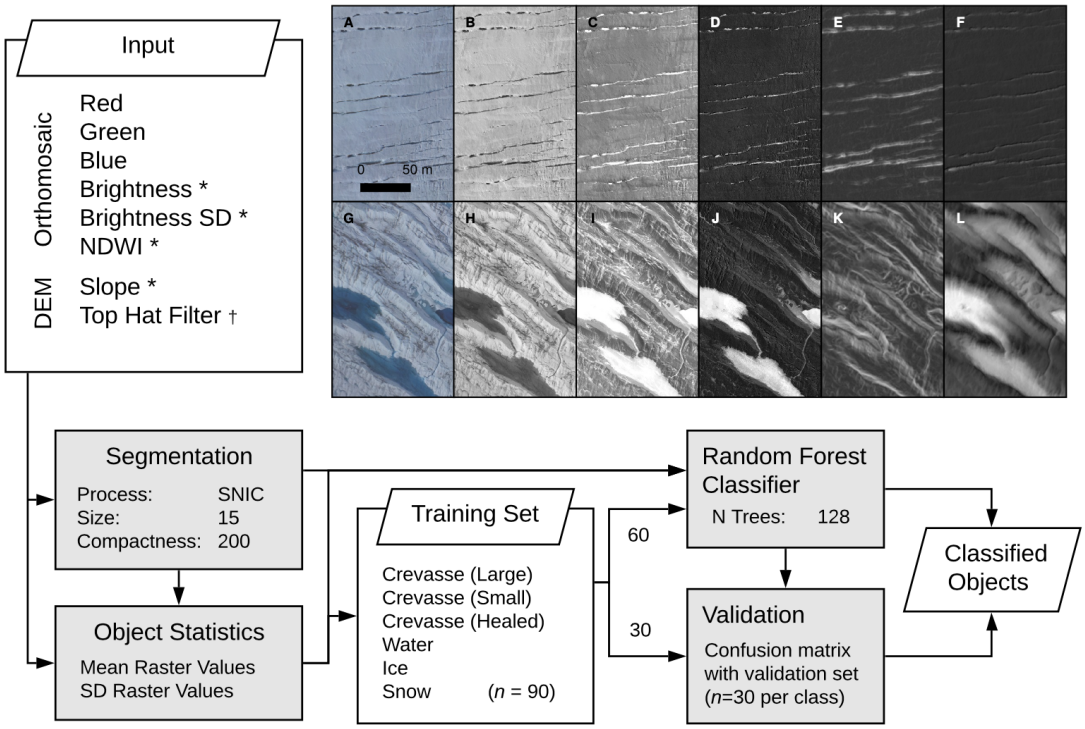

Figure S2. Flowchart of the method used to classify UAV imagery. Variables appended with an asterisk were calculated from input data within GEE, whilst the top hat filter, appended with a cross, was calculated separately in Matlab. Inset as for Figure 2 of main text, showing examples of OBIA input data for regions dominated by (a-f) small and (g-l) large crevasses. (a and g) RGB orthophotos. (b and h) Brightness. (c and i) Standard deviation of RGB values. (d and j) NDWI. (e and k) Slope, with hillshade overlaid. (f and l) Black-top-hat filtered DEM, with hillshade overlaid.

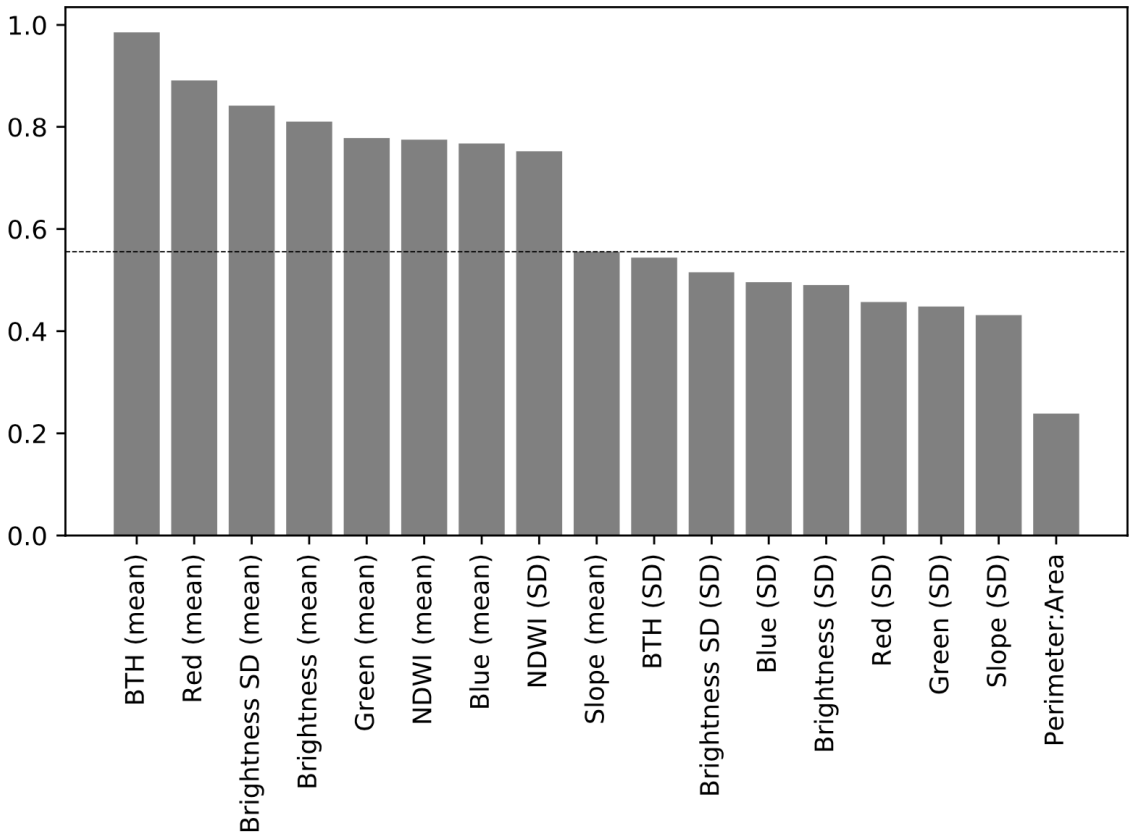

Figure S3. Results of mutual information tests for all potential input variables against training data. Median value is marked by the dotted line. BTH is black top-hat filter. SD is standard deviation.

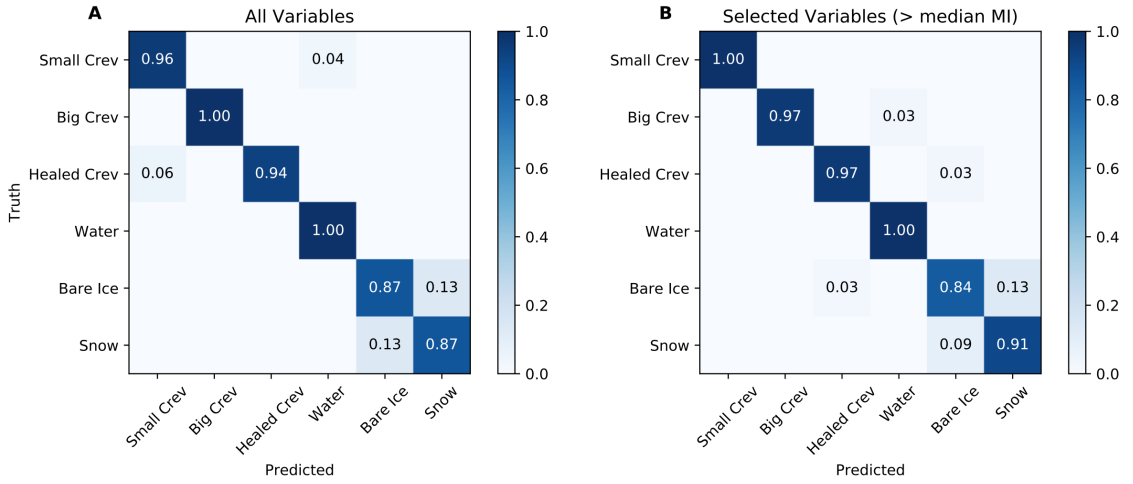

Figure S4. Normalised confusion diagrams for object-based image analysis of 2018-07-08 imagery for (A) all input variables; and (B) selected input variables with mutual information test results greater than median. For quantitative accuracy assessment of this data, see Table S2.

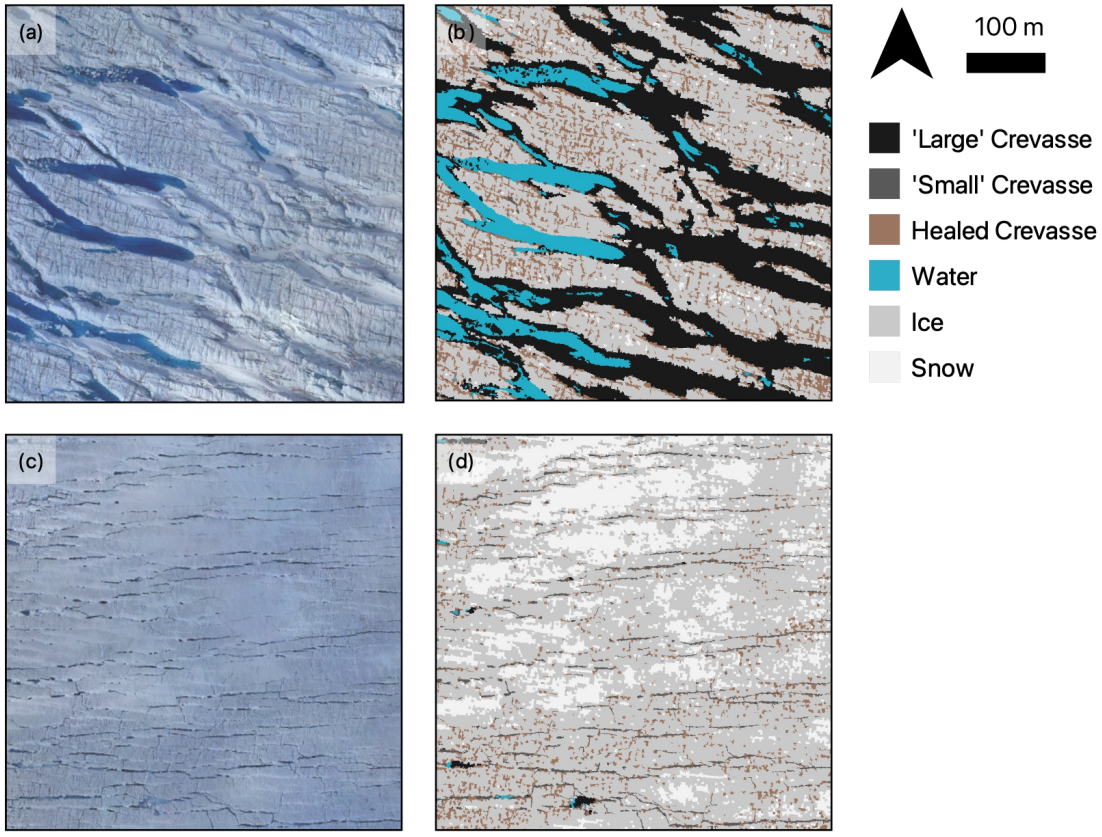

Figure S5. Example results for object-based image analysis of 2018-07-08 imagery. RGB and classified image for all six surface types shown for a region with 'large' (a, b) and 'small' (c, d) crevasses respectively.

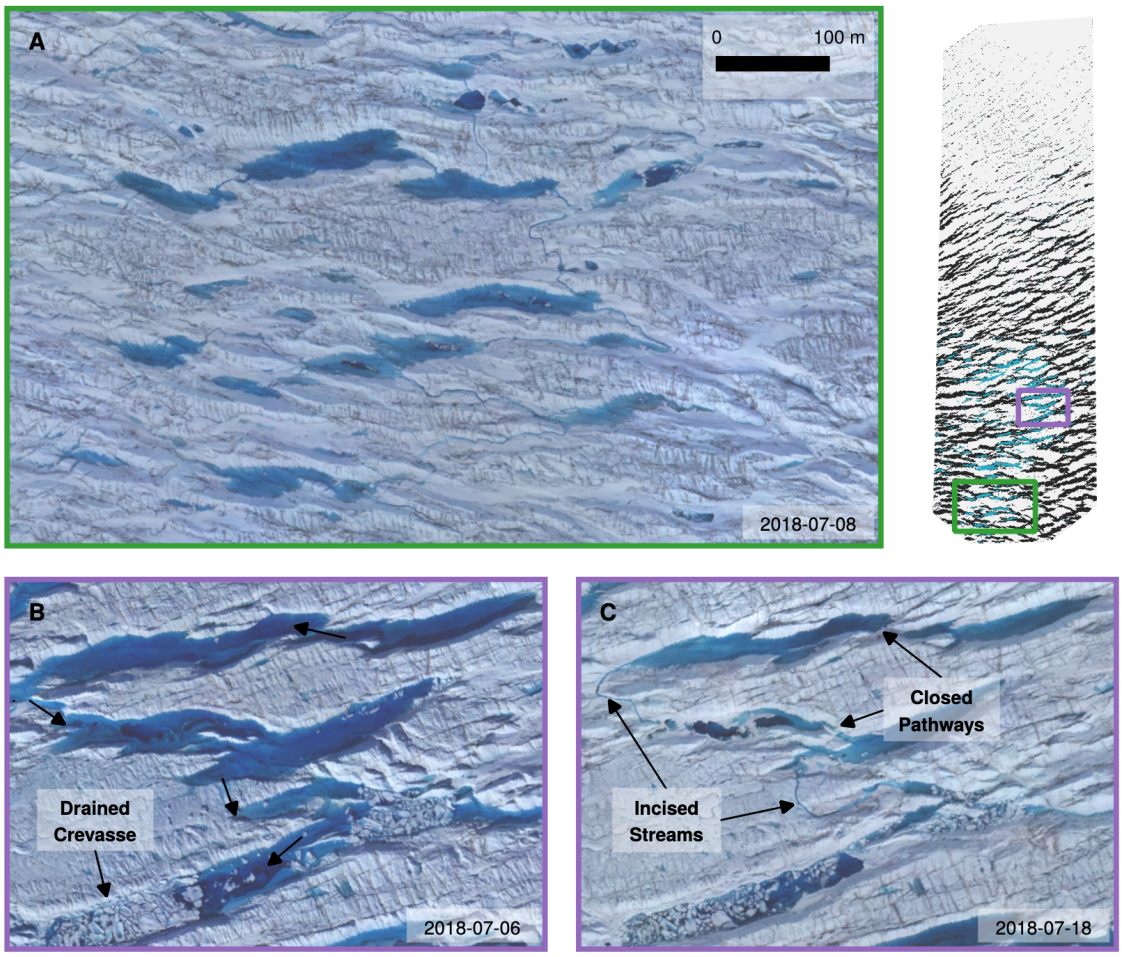

Figure S6. Supraglacial connections between crevasses. (A) Southwestern extent of UAV survey area, displaying clear incised supraglacial pathways between crevasses. (B–C) Crevasse system identified in main figure 7A–B in the 24 hours following (B) and 12 days following (C) drainage, showing the development of incised streams as water level lowers. Inset: subfigure extents identified in full UAV survey extent.

Figure S7. Evidence of significant lateral englacial flow channels at Store Glacier in July 2012. Channel occurs in a relict moulin (70° 33.497', -50° 05.912') located downstream of the rapidly draining Lake 028. (left) The englacial channel located within the relict moulin, with figure for scale. (right) View into the englacial channel. Although the moulin was no longer actively receiving melt, water (with a floating ice melange) existed in the channel. The endpoint was not visible.

Table S1. UAV survey date and times of flight midpoints (rounded to the nearest 5 minutes). All times in Coordinated Universal Time (UTC)

Survey Date	Time (UTC)
2018-07-05	21:10
2018-07-06	19:25
2018-07-07	17:25
2018-07-08	19:25
2018-07-18	14:20

Table S2. Accuracy assessment of random forest classification for 2018-07-08 survey, including calculated accuracy, precision, recall, F_1 score, and Matthew's Correlation Coefficient (MCC).

Class	Accuracy	Precision	Recall	F_1 Score	MCC
Small Crevasses	1	1	1	1	1
Large Crevasses	0.99	1	0.97	0.98	0.98
Healed Crevasses	0.99	1	0.97	0.98	0.98
Water	1	1	1	1	1
Bare Ice	0.95	0.89	0.84	0.86	0.83
Snow	0.96	0.86	0.91	0.89	0.86